

Dayside magnetopause reconnection and flux transfer events under radial interplanetary magnetic field (IMF): BepiColombo Earth-flyby observations

Weijie Sun, James A. Slavin, Rumi Nakamura, Daniel Heyner, Karlheinz J. Trattner, Johannes Z. D. Mieth, Jiutong Zhao, Qiu-Gang Zong, Sae Aizawa, Nicolas Andre, et al.

▶ **To cite this version:**

Weijie Sun, James A. Slavin, Rumi Nakamura, Daniel Heyner, Karlheinz J. Trattner, et al.. Dayside magnetopause reconnection and flux transfer events under radial interplanetary magnetic field (IMF): BepiColombo Earth-flyby observations. Annales Geophysicae, 2022, 40 (2), pp.217-229. 10.5194/angeo-40-217-2022 . insu-03672031

HAL Id: insu-03672031
https://insu.hal.science/insu-03672031

Submitted on 19 May 2022

HAL is a multi-disciplinary open access archive for the deposit and dissemination of scientific research documents, whether they are published or not. The documents may come from teaching and research institutions in France or abroad, or from public or private research centers.

L'archive ouverte pluridisciplinaire **HAL**, est destinée au dépôt et à la diffusion de documents scientifiques de niveau recherche, publiés ou non, émanant des établissements d'enseignement et de recherche français ou étrangers, des laboratoires publics ou privés.



Distributed under a Creative Commons Attribution| 4.0 International License

Ann. Geophys., 40, 217–229, 2022
https://doi.org/10.5194/angeo-40-217-2022
© Author(s) 2022. This work is distributed under
the Creative Commons Attribution 4.0 License.

Annales Geophysicae Open Access EGU

Dayside magnetopause reconnection and flux transfer events under radial interplanetary magnetic field (IMF): BepiColombo Earth-flyby observations

Weijie Sun[1], James A. Slavin[1], Rumi Nakamura[2], Daniel Heyner[3], Karlheinz J. Trattner[4], Johannes Z. D. Mieth[3], Jiutong Zhao[5], Qiu-Gang Zong[5], Sae Aizawa[6,7], Nicolas Andre[6], and Yoshifumi Saito[8]

[1]Department of Climate and Space Sciences and Engineering, University of Michigan, Ann Arbor, MI 48109, USA
[2]Space Research Institute, Austrian Academy of Sciences, Schmiedlstraße 6, 8042 Graz, Austria
[3]Institut für Geophysik und extraterrestrische Physik, Technische Universität Braunschweig, 38106 Braunschweig, Germany
[4]Laboratory for Atmospheric and Space Physics, University of Colorado, Boulder, CO 80303, USA
[5]School of Earth and Space Sciences, Peking University, Beijing 100871, China
[6]Institut de Recherche en Astrophysique et Planétologie, CNRS-UPS-CNES, Toulouse, France
[7]Department of Geophysics, Graduate School of Science, Tohoku University, Sendai, Japan
[8]Japan Aerospace Exploration Agency, Institute of Space and Astronautical Science, Kanagawa, Japan

Correspondence: Weijie Sun (wjsun@umich.edu)

Received: 20 October 2021 – Discussion started: 22 October 2021
Revised: 22 March 2022 – Accepted: 25 March 2022 – Published: 22 April 2022

Abstract. This study analyzes the flux transfer event (FTE)-type flux ropes and magnetic reconnection around the dayside magnetopause during BepiColombo's Earth flyby. The magnetosheath has a high plasma β (~ 8), and the interplanetary magnetic field (IMF) has a significant radial component. Six flux ropes are identified around the magnetopause. The motion of flux ropes together with the maximum magnetic shear model suggests that the reconnection X-line possibly swipes BepiColombo near the magnetic equator due to an increase in the radial component of the IMF. The flux rope with the highest flux content contains a clear coalescence signature, i.e., two smaller flux ropes merge, supporting theoretical predictions that the flux contents of flux ropes can grow through coalescence. The coalescence of the two FTE-type flux ropes takes place through secondary reconnection at the point of contact between the two flux ropes. The BepiColombo measurements indicate a large normalized guide field and a reconnection rate comparable to that measured at the magnetopause (~ 0.1).

1 Introduction

Flux transfer events (FTEs) are frequently observed near the outer boundaries, i.e., magnetopause, of planetary magnetospheres, including on Earth (e.g., Russell and Elphic, 1978; Saunders et al., 1984; Wang et al., 2005), Mercury (Russell and Walker, 1985; Slavin et al., 2009, 2010, 2012; Imber et al., 2014; Sun et al., 2020a; Zhong et al., 2020), Saturn (Jasinski et al., 2016, 2021), and Jupiter (Walker and Russell, 1985; Lai et al., 2012). Some of the FTEs have magnetic flux ropes at their cores, which consist of helical magnetic field lines surrounding stronger magnetic fields paralleling their central axes (Paschmann et al., 1982; Lee et al., 1993). These FTE-type flux ropes are created by multiple X-line reconnections in the magnetopause during intervals of significant magnetic shear across the magnetopause current sheet (Lee and Fu, 1985; Raeder, 2006). As a result, the FTE-type flux rope signal the occurrence of magnetic reconnection its direction of travel, can be used to infer the relative location of the reconnection X-line at the magnetopause.

The FTEs usually include magnetic field lines with one end connecting to the interplanetary magnetic field (IMF) and the other to a magnetospheric cusp. They transport magnetic flux from the dayside to the nightside magnetosphere

that drives the Dungey cycle in planetary magnetospheres with global intrinsic magnetic fields. Sun et al. (2022) recently reviewed the contributions of FTE-type flux ropes to the Dungey cycle in dipolar planetary magnetospheres. In Mercury's magnetosphere, FTE-type flux ropes transport the majority ($> 60\,\%$) of the circulated flux (Slavin et al., 2010; Sun et al., 2020a). In contrast, FTE-type flux ropes are estimated to transport only a small portion ($< 5\,\%$) of the circulated flux at Earth (Lockwood et al., 1995; Fear et al., 2017). For the giant outer planetary magnetospheres at Jupiter and Saturn, they appear to transport a negligible magnetic flux ($< 1\,\%$) for the solar wind-driven portion of their internal convection (Jasinski et al., 2021).

The FTEs on Earth's magnetosphere appear most frequently during periods of the southward IMF when the magnetic shear angle across the magnetopause is larger than 90° (e.g., Rijnbeek et al., 1984; Kuo et al., 1995; Wang et al., 2006). The locations of magnetopause X-lines are closely related to the orientation of the IMF. For example, during the purely southward IMF, reconnection most likely occurs on the magnetopause near the subsolar point (Dungey, 1961). During the purely northward IMF, reconnections occur on the magnetopause tailward of the cusp (Dungey, 1961; Song and Russell, 1992; Shi et al., 2009, 2013; Gou et al., 2016). Magnetic reconnection is also thought to occur at the dayside magnetopause under the strong radial IMF (B_x dominate) (Belenkaya, 1998; Luhmann et al., 1984; Pi et al., 2017; Tang et al., 2013; Toledo-Redondo et al., 2021), but the strong radial IMF conditions are less well studied.

Coalescence, which refers to the merging of neighboring flux ropes, is thought to be an important process in space plasma physics (Biskamp and Welter, 1980; Dorelli and Bhattacharjee, 2009; Fermo et al., 2011; Hoilijoki et al., 2017). The merging of flux ropes is associated with secondary reconnection, and changes in magnetic field configuration caused by this secondary reconnection can energize particles, especially electrons (Drake et al., 2006). Furthermore, several studies have suggested that FTE-type flux ropes are initially formed between electron and ion scales. They then grow through coalescence, thereby increasing their magnetic flux contents and scales (Fermo et al., 2011; Akhavan-Tafti et al., 2018). NASA's Magnetospheric Multiscale (MMS) Mission (Burch et al., 2016) has provided several observations of secondary reconnections between neighboring flux ropes (see Zhou et al., 2017), between flux ropes and Earth's dipole magnetic field (Poh et al., 2019), and between interlinked flux tubes (Øieroset et al., 2016; Kacem et al., 2018).

This study investigates FTE-type flux ropes and reconnection at Earth's dayside magnetopause during BepiColombo's flyby on 10 April 2020. The paper is arranged as follows. Section 2 introduces the BepiColombo mission and the measurements during Earth's dayside magnetopause crossing. Section 3 analyzes the distribution of magnetopause reconnection with a strong radial IMF component and the properties of the flux ropes, including a coalescence event. Section 4 provides a summary of our results.

2 BepiColombo dayside magnetopause crossing

2.1 Spacecraft and instrumentation

BepiColombo is a joint mission by the European Space Agency (ESA) and Japan Aerospace Exploration Agency (JAXA), which consists of two spacecraft named the Mercury Planetary Orbiter (MPO) and Mercury Magnetospheric Orbiter (MMO or Mio). These spacecraft together aim to carry out detailed investigations of Mercury's interior, surface, exosphere, and magnetosphere (Milillo et al., 2020; Murakami et al., 2020; Benkhoff et al., 2010). The mission made its first planetary flyby maneuver at Earth on 10 April 2020 (Mangano et al., 2021), during which several instruments collected measurements. The MPO and the MMO were attached during the Earth flyby, and therefore their measurements could be deemed one observation point. The two spacecraft will be separated when they are scheduled to insert into Mercury's orbit by late 2025 or early 2026.

This study uses measurements collected by the magnetometer (MAG) onboard MPO (Heyner et al., 2021) and the low-energy electron by the Mercury Electron Analyzer (MEA) (Sauvaud et al., 2010), which is part of the Mercury Plasma Particle Experiment (MPPE) onboard MMO (Saito et al., 2021). The MPO/MAG includes one outboard sensor and one inboard sensor, and it has a sampling rate of 128 Hz. Mio/MEA has a sampling rate of 4 s. The IMF and solar wind conditions are obtained from the OMNI dataset (King and Papitashvili, 2005), which has a time resolution of 1 min.

2.2 Overview of the magnetosheath and magnetopause

Figure 1 shows an overview of the dayside magnetopause crossing during BepiColombo's Earth flyby. BepiColombo traveled from the magnetosheath into the dayside magnetosphere. It crossed the magnetopause at a distance of $\sim 4.8\,R_E$ (R_E is 1 Earth radius) dawnward from the subsolar magnetopause, which corresponded to a position of (11.2, −4.8, −0.3) R_E in the geocentric solar magnetospheric (GSM) coordinate. During the 30 min interval around the magnetopause crossing ($\sim$ 00:05 to 00:35 UT) analyzed here, the IMF was southward with a strong radial component; i.e., the B_x was the dominant component ($B_x/B_t > 0.7$ in Fig. 1h). The average electron density in the magnetosheath was estimated to be $\sim 10\,\mathrm{cm}^{-3}$ based on the onboard-calculated partial moment from Mio/MEA between 00:05 and 00:28 UT. The magnetosheath plasma β was high, with a value of ~ 8.0, which was the ratio of the thermal pressure to the magnetic pressure. The thermal pressure in the magnetosheath was calculated by assuming that the pressure balance existed across the dayside magnetopause and that the thermal pressure in-

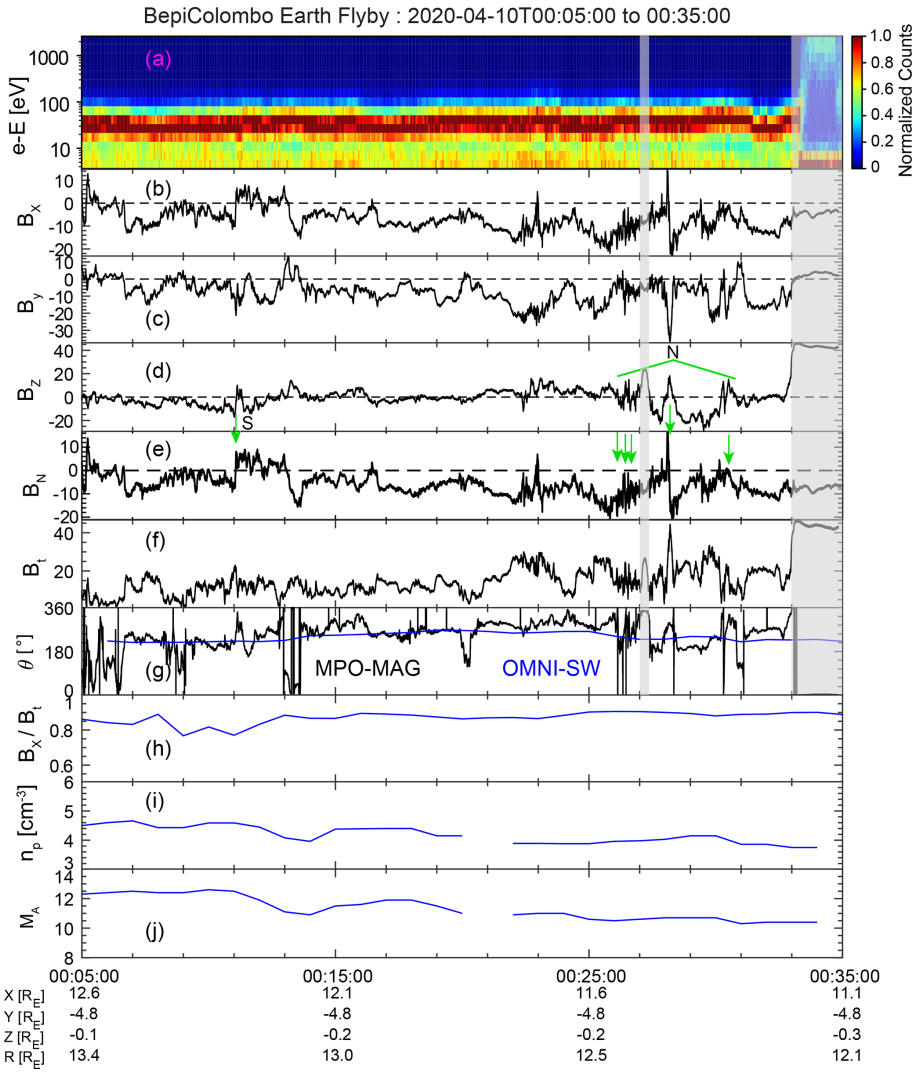


Figure 1. The electrons and magnetic field measurements of the dayside magnetopause during BepiColombo's Earth flyby. **(a)** The time–energy spectrogram of normalized electron counts from Mio/MEA, **(b)** magnetic x component B_x, **(c)** y component B_y, **(d)** z component B_z, **(e)** magnetic component normal to the magnetopause B_N, **(f)** magnetic field intensity B_t, **(g)** clock angle (θ), **(h)** B_x/B_t of the IMF, **(i)** solar wind number density (n_p), and **(j)** solar wind Alfvénic Mach number (M_A). All quantities are in the geocentric solar magnetospheric (GSM) coordinate. The green arrows in panel **(e)** indicate the six FTE-type flux ropes. "S" indicates southward traveling and "N" northward traveling. The θ in panel **(g)** is defined as $\arctan(B_y/B_z)$, ranging from 0 to 360°. In panel **(g)**, the black line is from the measurements of MPO/MAG, and the blue line is from OMNI.

side the dayside magnetosphere was negligible compared to the magnetic pressure.

3 Magnetopause reconnections and FTE-type flux ropes

3.1 Identification of FTE-type flux ropes

The FTE-type flux ropes were identified after the measured magnetic field was rotated into boundary normal coordinates (the LMN coordinate). The minimum variance analysis (MVA) (Sonnerup and Cahill, 1967; Sonnerup and Scheible, 1998) was performed on the magnetic field measurements across the magnetopause current sheet from 00:32:30 to 00:33:25 UT to obtain the LMN coordinate. The MVA results produced L = [0.10, 0.24, 0.97] (maximum variance direction), M = [0.12, 0.96, −0.25] (intermediate variance direction), and N = [0.99, −0.14, −0.06] (minimum variance direction), and the eigenvalue ratios were $\lambda_{max}/\lambda_{int} \sim 54.3$ and $\lambda_{int}/\lambda_{min} \sim 3.9$. The λ_{max}, λ_{int} and λ_{min} are the maximum, intermediate, and minimum eigenvalues. Both of the ratios were larger than 3, indicating that the LMN coordinate of the magnetopause was well determined (Sonnerup and Scheible, 1998).

Table 1. List and properties of FTE-type flux ropes observed during BepiColombo's dayside magnetopause crossing.

No.	Time	Duration (s)	Traveling direction	Core field intensity (nT)	Scale (km)[b]	Flux content (kWb)	X^2
1	00:11:04	∼ 12	Southward	–[a]	–	–	–
2	00:26:06	∼ 7	Northward	∼ 23.9	462, 388 (0.84)	∼ 13.7	∼ 0.04
3	00:26:26	∼ 6	Northward	∼ 60.8	565, 524 (0.93)	∼ 22.5	∼ 0.04
4	00:26:35	∼ 4	Northward	–	–	–	–
5	00:28:13	∼ 20	Northward	∼ 41	1745, 1281 (0.73)	∼ 300	∼ 0.08
6	00:30:26	∼ 15	Northward	∼ 45.2	1853,1745 (0.94)	∼ 188	∼ 0.08

[a] "–" indicates that the values are not determined by the flux rope model. See the text for more information on the flux rope modeling. [b] scale contains semi-minor and semi-major, and the ratio between semi-minor and semi-major refers to the flattened profile. See the text for more information.

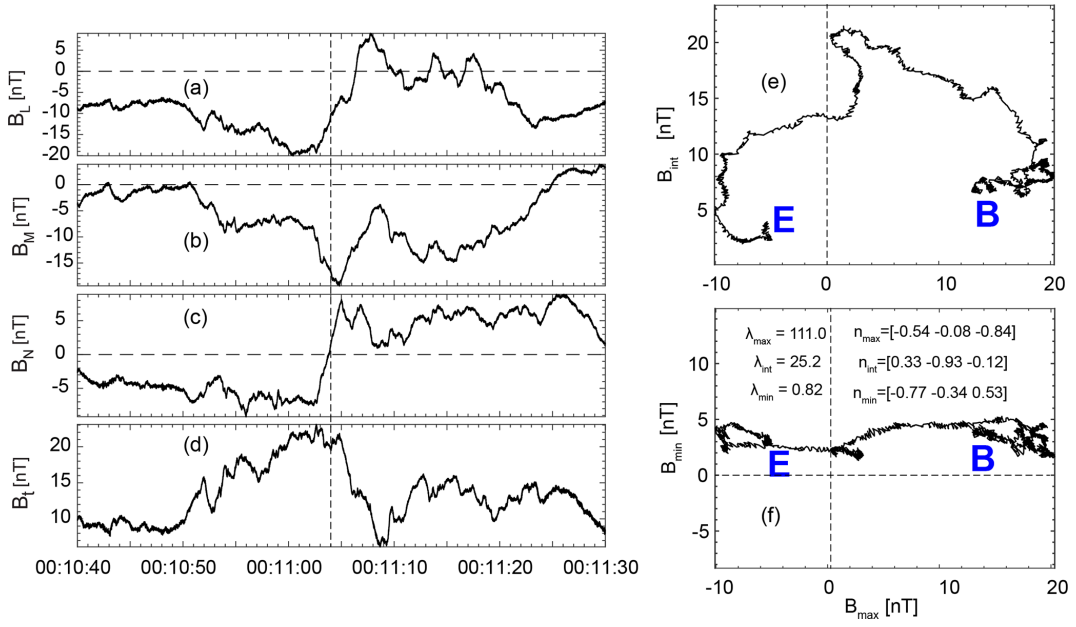


Figure 2. The southward-traveling FTE-type flux rope centered at ∼ 00:11:04 UT. **(a)** Magnetic field component in the L direction, B_{L}, **(b)** magnetic field component in the M direction, B_{M}, **(c)** magnetic field component in the N direction, B_{N}, and **(d)** B_{t}. This LMN is the local coordinate of the magnetopause. Panels **(e)** and **(f)** are the hodograms of the magnetic field measurements under the local coordinate of the flux rope. "B" and "E" indicate the beginning and end of the data points.

The FTE-type flux ropes were identified with bipolar signatures in the normal magnetic field (B_{N}) and clear magnetic field rotation (Russell and Elphic, 1978). The identification of flux ropes also required the signature of a strong magnetic field along their central axis, i.e., the intermediate variance direction (see Fig. 2 for an example and, e.g., Slavin et al., 2009; Akhavan-Tafti et al., 2018). Six FTE-type flux ropes were identified in this manner in the magnetosheath just upstream of the dayside magnetopause and are marked with green arrows in Fig. 1e and listed in Table 1.

The first possible FTE-type flux rope shown in Fig. 2 was centered at ∼ 00:11:04 UT when the IMF clock angle was ∼ 210°, and B_x/B_{t} was ∼ 0.75. This flux rope traveled southward, as inferred from the polarities of the B_{N} variation (negative to positive, Fig. 2c). The flux rope corresponded to clear enhancement in B_{M} (Fig. 2b) and field rotation in the plane of $B_{\mathrm{max}} - B_{\mathrm{int}}$ (Fig. 2e). However, the enhancement in the B_{t} strength preceding the reversal in B_{N} could indicate that the magnetic flux was piled up or that this structure was a magnetosheath structure other than a flux rope. About 2 min later, the clock angle increased to ∼ 260°. This IMF orientation persisted for about 12 min, during which no FTE-type flux ropes were observed. At ∼ 00:26:06 UT, the clock angle decreased from ∼ 260° to ∼ 210°, while the ratio of B_x/B_{t} increased to ∼ 0.90. At this point, five FTE-type flux ropes successively appeared up to the point where the magnetopause was crossed. The traveling direction for these five flux ropes was inferred to be northward, again based on the B_{N} variations. The first flux rope traveled southward, indicating that the primary magnetopause X-line was initially located north-

ward of the spacecraft. Later, the northward motion of the five flux ropes indicated that the primary magnetopause X-line(s) had shifted southward.

3.2 Reconnection X-lines from the maximum magnetic shear model

To further investigate reconnection during BepiColombo's dayside magnetopause traversal, the maximum magnetic shear model (Trattner et al., 2007, 2017) was employed to deduce the locations of reconnection X-lines. The magnetic shear angle plots during the intervals centered at 00:09, 00:20, and 00:28 UT are shown in Fig. 3. Figure 3a and b correspond to a distorted feature of the anti-parallel reconnection region, which has recently been termed a "Knee" event (Trattner et al., 2021). The bent shape of the anti-parallel reconnection region is associated with the field line draping in the magnetosheath during the dominant B_x (significantly sunward) component in this period. Figure 3c did not provide the predicted X-line. This was because a continuous X-line along the maximum magnetic shear location was difficult to obtain under the situation of a $B_x/B_t \geq 0.9$, which was due to the lack of a comprehensive study on how the significant radial IMF draping around the magnetopause influences magnetic reconnection.

In Fig. 3a, BepiColombo was located southward of the predicted X-line. From Fig. 3a to b, the predicted X-line crossed the location of BepiColombo and was then located to the south of BepiColombo. The changes in X-line locations from Fig. 3a to b were due to the IMF clock angle decreasing around 10° together with the B_x/B_t increasing from 0.78 to 0.86.

The traveling directions for the FTE-type flux ropes were consistent with the predicted locations of the reconnection X-line by the maximum magnetic shear model during the changing solar wind conditions for this magnetopause encounter. Figure 3a corresponded to the only southward-traveling FTE-type flux rope, while the other five northward-traveling FTE-type flux ropes were observed during the conditions shown in Fig. 3b and c. It needs to be noted that the FTE-type flux ropes and reconnection exhausts should correspond to strong lateral motion as the predicted X-lines were significantly along the north–south direction. The reconnection exhausts would correspond to a strong duskward component when the spacecraft was located southward of the X-line and a strong dawnward component when it was northward of the X-line. Although the maximum magnetic shear model faces challenges in determining the draping magnetic field lines in the magnetosheath during the intervals of the dominant B_x component (Trattner et al., 2007, 2012), the model predictions are consistent with our observations during BepiColombo's crossing.

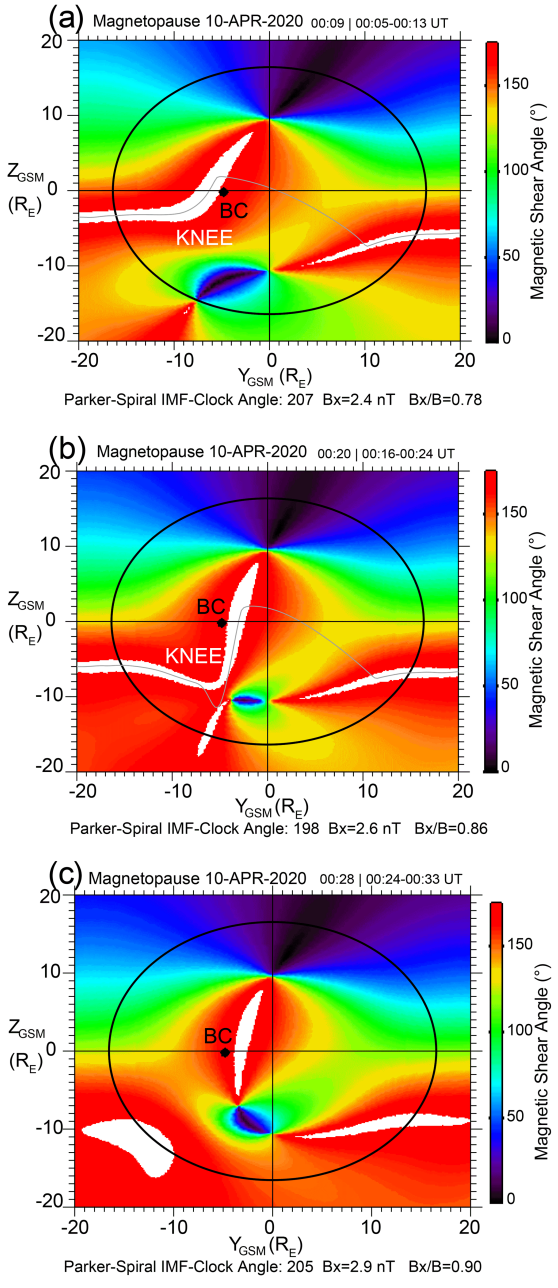


Figure 3. Magnetic shear angle plots on the magnetopause surface during BepiColombo's dayside magnetopause crossing, which are obtained through the maximum magnetic shear model (Trattner et al., 2007). Panels **(a–c)** correspond to the IMF averaged from 00:05 to 00:13 UT, 00:16 to 00:24 UT, and 00:24 to 00:33 UT, respectively. The black circle represents the terminator plane separating the dayside magnetopause from the tailward magnetopause. The grey line represents the predicted magnetopause reconnection line. White areas correspond to the magnetic shear angle within 3° of 180°. The black dots are the location of BepiColombo ("BC"). In panel **(c)**, the predicted X-line is not provided. This is because a continuous X-line along the maximum magnetic shear location is difficult to obtain under the situation of a $B_x/B_t \geq 0.9$.

3.3 FTE-type flux rope modeling

This study employed a force-free flux rope model (Kivelson and Khurana, 1995) to fit the FTE-type flux ropes. This flux rope model starts from the periodic pinch solution (Schindler et al., 1973) of Ampere's law ($\nabla \times \boldsymbol{B} = \mu_0 \boldsymbol{J}$), where $\boldsymbol{B}$ is the magnetic field vector, $\boldsymbol{J}$ is the current density vector, and μ_0 is the magnetic permeability in a vacuum. Kivelson and Khurana (1995) further include the axial magnetic field component ($B_{\rm int}$) in the periodic pinch solution. The flux rope model introduced by Kivelson and Khurana (1995) does not consider the gradient of the magnetic field along the axis of the flux rope. The self-consistent solution of the flux rope model is

$$\begin{cases} B_{\rm max} = \left(\frac{B_{\rm T}}{\chi}\right)\sqrt{1+\epsilon^2}\sinh\left(\frac{x_{\rm min}}{T}\right), \\ B_{\rm int} = \left(\frac{B_{\rm T}}{\chi}\right)\sqrt{1+\left(\frac{B_{\rm int0}\chi}{B_{\rm T}}\right)^2}, \\ B_{\rm min} = \left(\frac{B_{\rm T}}{\chi}\right)\epsilon\sin\left(\frac{x_{\rm max}}{T}\right). \end{cases} \quad (1)$$

In the equation, $x_{\rm min}$ and $x_{\rm max}$ are the positions in the flux rope along the directions of $\boldsymbol{n}_{\rm min}$ and $\boldsymbol{n}_{\rm max}$. $\boldsymbol{n}_{\rm min}$, $\boldsymbol{n}_{\rm int}$, and $\boldsymbol{n}_{\rm max}$ refer to the local coordinate of the flux rope, which are determined from the MVA on the flux rope. T is the vertical scale of the flux rope in the $\boldsymbol{n}_{\rm max}$ direction, and $B_{\rm T}$ is the magnetic field intensity near the boundary of the flux rope along the $\boldsymbol{n}_{\rm min}$ direction. $B_{\rm int0}$ is $B_{\rm int}$ in the background. χ is

$$\chi = \epsilon\cos\left(\frac{x_{\rm max}}{T}\right) + \sqrt{1+\epsilon^2}\cosh\left(\frac{x_{\rm min}}{T}\right). \quad (2)$$

In this equation, the parameter ε is associated with the shape of the flux rope, i.e., from flattened to circular profiles. The axial flux content ($\Phi_{\rm axial}$) is calculated by integrating the axial field ($B_{\rm int}$) over the entire flux rope area:

$$\Phi_{\rm axial} = \int B_{\rm int}{\rm d}S. \quad (3)$$

During the fitting, we assume that the traveling speed of flux ropes was 100 km s^{-1}, which corresponds to the average Alfvén speed in the subsolar magnetosheath. The traveling speed is required in calculating the scales and magnetic flux content for the flux ropes. Least squares of the minimization of the magnetic field differences (X^2) is employed to define the best fit, which is calculated from

$$X^2 = \frac{\sum_{i=1}^{N_{\rm point}}\sum_{j}^{\rm max,int,min}\left[\left(B_j(i) - B'_j(i)\right)/B_{\rm t}(i)\right]^2}{N_{\rm point}}, \quad (4)$$

where $B_{\rm max}$, $B_{\rm int}$, $B_{\rm min}$, and $B_{\rm t}$ are the components and magnitude of the measured magnetic fields and $B'_{\rm max}$, $B'_{\rm int}$, and $B'_{\rm min}$ are the components of the magnetic fields from the model. $N_{\rm point}$ is the number of data points. We set up a threshold of $X^2 < 0.1$ to be the successful modeling.

Differently from the circular profile of flux ropes resulting from the Lundquist force-free flux rope model (Lundquist, 1950; Burlaga, 1988; Lepping et al., 1990), this force-free model can result in either flattened or circular profiles of flux ropes. We use "semi-minor" and "semi-major" to refer to the flattened features. Semi-major corresponds to the scale of flux rope along the $\boldsymbol{n}_{\rm min}$ direction, which is close to the L direction of the magnetopause. Semi-minor corresponds to the scale of flux rope along the $\boldsymbol{n}_{\rm max}$ direction, which is close to the N direction of the magnetopause. This flux rope model is successfully applied for the flux ropes in Earth's plasma sheet (Kivelson and Khurana, 1995), on Earth's magnetopause (Zhang et al., 2008), and in Mercury's plasma sheet (Zhao et al., 2019).

Out of the six FTE-type flux ropes, four were successfully modeled. As an example, the modeling curves of the flux rope centered at 00:28:13 UT are shown in Fig. 4a–d. In the figures, the dashed lines overlapping with the solid measured magnetic fields represent the modeling curves from the flux rope model. It can be seen clearly that the two curves are close to each other, and this flux rope is well fitted by the model. The modeling results for our flux ropes are summarized in Table 1. The plasma density of $\sim 10\,{\rm cm}^{-3}$ in the magnetosheath corresponds to an ion inertial length ($d_{\rm i}$) of ~ 70 km. The two FTE-type flux ropes at 00:26:06 UT and 00:26:26 UT are on the scales of several $d_{\rm i}$. The magnetic flux contents of these two flux ropes are small (~ 20 kWb). In addition, these two flux ropes correspond to the largest and smallest core fields. The other two FTE-type flux ropes at 00:28:13 UT and 00:30:26 UT are on the scales of more than 10 $d_{\rm i}$. These two flux ropes contain much higher magnetic flux (~ 300 and ~ 188 kWb). The analysis of the flux rope at $\sim$ 00:28:13 UT corresponding to the highest magnetic flux content is shown in the next section. Moreover, the flux ropes at 00:26:06 UT, 00:26:26 UT, and 00:30:26 UT are close to circular profiles with the semi-minor slightly smaller than the semi-major. The flux rope at $\sim$ 00:28:13 UT corresponds to the most flattened profile.

3.4 Coalescence event

Figure 4a–d show the magnetic field measurements of the FTE-type flux rope centered at $\sim$ 00:28:13 UT in the LMN coordinate. This FTE-type flux rope corresponds to the fifth green arrow counting from the left-hand side in Fig. 1e. Figure 4c showed that the $B_{\rm N}$ included two successive bipolar signatures, which implied that two smaller-scale flux ropes were merging. Indeed, the hodogram in the $B_{\rm max}$-$B_{\rm int}$ plane in Fig. 4f confirmed the field rotations of two flux ropes, named "FR#A" and "FR#B". Figure 4e further illustrated the merging of the two flux ropes and the trajectory of BepiColombo. The magenta arrow and shaded region in Fig. 4e indicated the possible secondary reconnection between FR#A and FR#B. This FTE-type flux rope with the highest flux content possibly resulted from the coalescence of two smaller-scale flux ropes.

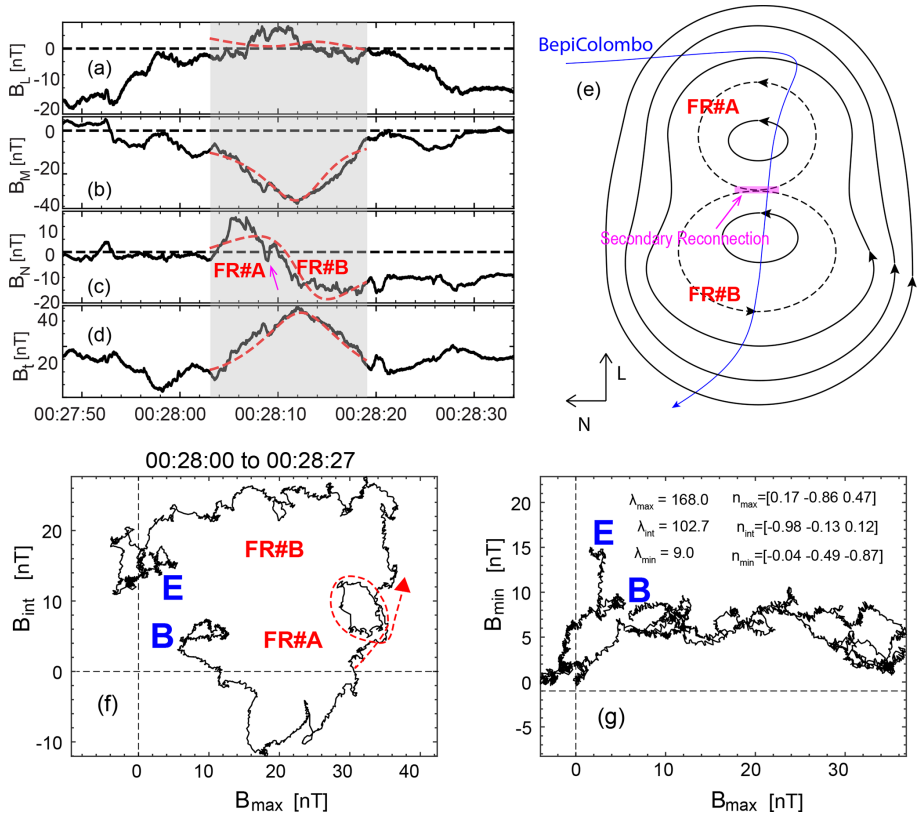


Figure 4. Overview of the flux rope centered at ∼ 00:28:13 UT with the coalescence feature. **(a)** B_L, **(b)** B_M, **(c)** B_N, and **(d)** B_t. The dashed lines are obtained from the flux rope model. This LMN is the local coordinate of the magnetopause. See the text for more information. **(e)** An illustration of the coalescence event and BepiColombo's trajectory. The secondary reconnection site is marked by the magenta region. Panels **(f)** and **(g)** are the hodograms of the magnetic field measurements under the local coordinate of the flux rope. "B" and "E" indicate the beginning and end of the data points. FR#A and FR#B indicate two flux ropes.

In order to study how well aligned FR#A and FR#B were, we applied the MVA to FR#A from 00:28:03 to 00:28:09 and FR#B from 00:28:09 to 00:28:16 separately. The eigenvalue ratios were $\lambda_{max}/\lambda_{int} \sim 1.91$ and $\lambda_{int}/\lambda_{min} \sim 21.7$ for FR#A. The eigenvalue ratios were $\lambda_{max}/\lambda_{int} \sim 3.34$ and $\lambda_{int}/\lambda_{min} \sim 12.6$ for FR#B. The large values of $\lambda_{int}/\lambda_{min}$ indicated that the $\boldsymbol{n}_{min}$ were well determined for both flux ropes. $\boldsymbol{n}_{min}$ was [−0.20, −0.58, −0.79] for FR#A, and $\boldsymbol{n}_{min}$ was [0.23, −0.55, −0.80] for FR#B. The $\boldsymbol{n}_{min}$ values were close to each other, with a separation angle of 25°. The $\boldsymbol{n}_{min}$ obtained for the coalescence event was [−0.04, −0.49, −0.87], which was 12 and 17° away from the $\boldsymbol{n}_{min}$ of FR#A and FR#B separately. The small separations of $\boldsymbol{n}_{min}$ should indicate that FR#A and FR#B were well aligned. It needs to be noted that the coalescence signature was only observed in this FTE-type flux rope centered at ∼ 00:28:13 UT. The successive bipolar signatures of B_N were not found in the other five FTE-type flux ropes.

3.5 Magnetopause reconnection and secondary magnetic reconnection

In Fig. 5, the properties of the secondary current sheet in the coalescence event and the magnetopause current sheet are studied. For the secondary current sheet, the eigenvalue ratios were $\lambda_{max}/\lambda_{int} \sim 6.4$ and $\lambda_{int}/\lambda_{min} \sim 11.0$, resulting from the MVA. Both of the eigenvalue ratios were larger than 3, indicating that the local coordinate of the secondary current sheet was well established. The magnetic field measurements of the magnetopause current sheet were shown in the LMN coordinate.

In the reconnecting current sheet, the dimensionless reconnection rate can be determined from the ratio of the normal magnetic field component (B_{normal}) to the reconnecting magnetic field (B_{inflow}) in the inflow region (Sonnerup, 1974; Sonnerup et al., 1981; Fuselier and Lewis, 2011; Phan et al., 2001; Sun et al., 2020b). In the secondary current sheet (Fig. 5a–d), B_{normal} was ∼ 5 nT, which corresponded to B_{min} averaged from 00:28:08.8 to 00:28:09.6 UT. Here the average B_t from 00:28:09.8 to 00:28:10.4 UT was taken as the B_{inflow} (∼ 36 nT). The dimensionless reconnection rate was ∼ 0.14

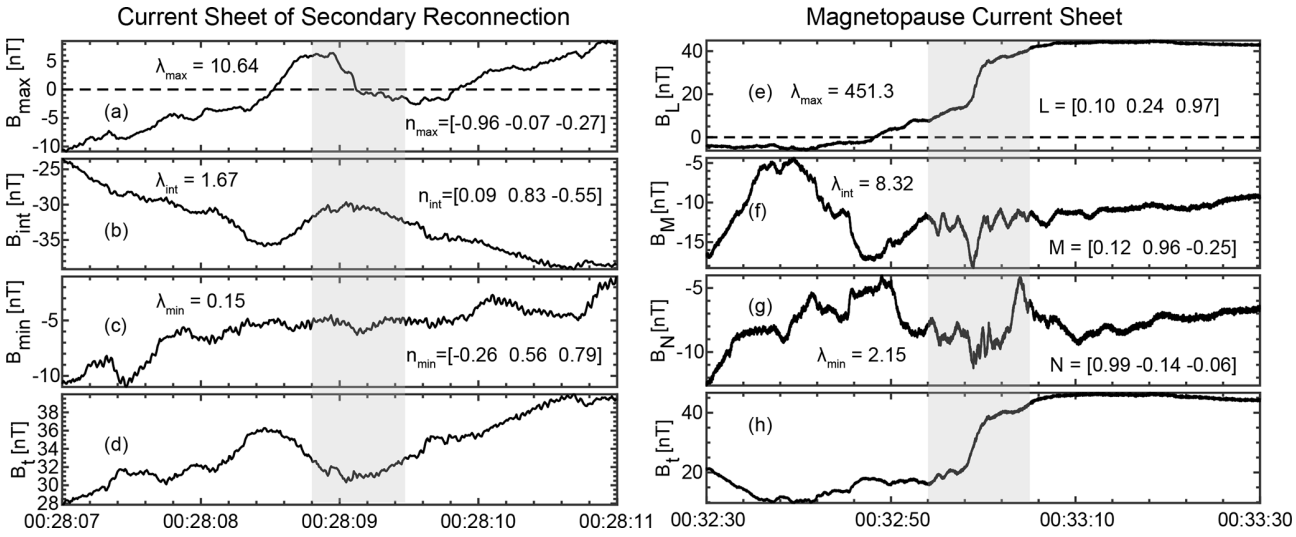


Figure 5. The magnetic field measurements under their separately local coordinate for the reconnecting current sheet of the coalescence event and the magnetopause current sheet. Panels **(a)** to **(d)** are for the secondary current sheet of the coalescence event. $\boldsymbol{n}_{\min}$, $\boldsymbol{n}_{\text{int}}$, and $\boldsymbol{n}_{\max}$ refer to the local coordinate of the secondary current sheet. Panels **(e)** to **(h)** are for the magnetopause current sheet. The LMN local coordinate of the magnetopause current sheet is used. The eigenvalues and corresponding eigenvectors result from the MVA.

if the reconnection occurred in the secondary current sheet. Meanwhile, the intensity of the guide field (B_{int}, Fig. 5b) was ~ 32 nT across the current sheet, which was ~ 0.89 when normalized to B_{inflow}. In the magnetopause current sheet, B_{normal} was 8.3 nT, which corresponded to the averaged B_{N} from 00:32:56 to 00:33:05 UT (Fig. 5g). B_{inflow} on the magnetosphere side adjacent to the magnetopause was ~ 46.1 nT, which corresponded to the averaged B_{t} from 00:33:06 to 00:33:15 UT (Fig. 5h). Thus, the dimensionless reconnection rate was calculated to be ~ 0.18. The guide field across the magnetopause was ~ 13 nT (B_{M}, Fig. 5f), which was 0.28 normalized to B_{inflow}.

However, it needs to be pointed out that the estimation of the reconnection rate based on $B_{\text{N}}/B_{\text{inflow}}$ could be imprecise. For example, the uncertainties of the normal direction and the fluctuations in the field strength could influence the accuracy of the reconnection rates. As noted by Sonnerup and Scheible (1998) and Khrabrov and Sonnerup (1998), there were uncertainties in the eigenvectors determined by the MVA, which could be either statistical error or error due to the magnetic structure not being perfectly stationary and one-dimensional. By employing the method introduced by Khrabrov and Sonnerup (1998), we obtained an uncertainty of ~ 0.93 nT for the B_{normal} of the secondary current sheet and ~ 0.04 nT for the magnetopause current sheet.

Furthermore, it was not certain that magnetic reconnection was occurring in the secondary current sheet or the magnetopause current sheet when BepiColombo crossed them. There was no complementary evidence of the magnetic reconnection since the measurements from BepiColombo were limited during the Earth flyby. The low-energy electron measurements (Mio/MEA) were limited in the field of view, and the time resolution was ~ 4 s. The MEA could not provide a complete distribution relative to the background magnetic field, and its time resolution was much longer than the timescale of the secondary current sheet. Therefore, the conclusions obtained about magnetic reconnection are tentative and further analysis about a similar event is needed, especially those measurements taken from the MMS.

4 Conclusions and discussions

Our analysis of the subsolar magnetopause observations during BepiColombo's Earth flyby has produced several conclusions.

First, BepiColombo's dayside magnetopause crossing took place during an interval when the magnetosheath had a high plasma β (~ 8) and the IMF had a strong radial component ($B_x/B_{\text{t}} > 0.7$). The traveling of the FTE-type flux rope suggests that the X-line crosses the location of BepiColombo. Although there is a possibility that the first and only southward-traveling FTE-type flux rope is a magnetosheath structure, the predictions of the maximum magnetic shear model suggest that the X-line crosses the location of BepiColombo as well. The X-line motion is associated with the rotation and the x component increase in the IMF. BepiColombo crosses the magnetopause near the magnetic equator, and 10 April 2020 is close to the spring equinox, which indicates a small influence of Earth's dipole tilt. These observations of the possible crossing of the X-line provide clear evidence of magnetic reconnection occurrence near the magnetic equator under a strong radial IMF.

Second, the properties of the FTE-type flux ropes are obtained by employing a force-free flux rope model introduced by Kivelson and Khurana (1995). The FTE-type flux ropes correspond to scales ranging from several d_i to around 20 d_i, and the FTE-type flux rope with a large scale and the highest magnetic flux content exhibits clear coalescence signatures. These observations strongly support the theories in which the FTE-type flux ropes grow in scale and magnetic flux content through coalescence.

Third, magnetic reconnection in the coalescence event and the magnetopause current sheet is investigated. The reconnection rate of the secondary reconnection (0.14) is comparable to the reconnection rate of the dayside magnetopause (0.18). The secondary reconnection corresponds to a large normalized guide field (0.89) and the magnetopause reconnection to a moderate guide field (0.28). However, there is no complementary evidence that magnetic reconnection is occurring in the secondary current sheet and magnetopause current sheet. Therefore, the conclusions about magnetic reconnection are tentative.

The large guide field of the secondary magnetic reconnection during the coalescence observed by BepiColombo is likely a common feature. For example, Zhou et al. (2017) reported a coalescence event with a strong guide field. We suggest that these large guide fields should be included in future simulations, which investigate the particle energizations due to coalescence. The large guide fields may influence the reconnection rate, as suggested by Pritchett and Coroniti (2004) and Ricci et al. (2004), and therefore affect the energization of particles during the coalescence. Furthermore, a recent investigation also suggests that a large guide field might limit the ability of Fermi acceleration during the coalescence (Montag et al., 2017).

Finally, the FTE-type flux rope containing the coalescence signature has a scale of ~ 20 d_i. Therefore, the secondary reconnecting current sheet embedded within the FTE-type flux rope likely has a scale smaller than 20 d_i. We want to note that the secondary reconnection during the coalescence of flux ropes shares some similarities with the electron-only reconnection associated with the magnetosheath turbulence, whose reconnecting current sheet has scales smaller than 10 d_i and is accompanied by a large guide field as revealed by MMS measurements (Phan et al., 2018; Stawarz et al., 2019) and simulations (Califano et al., 2020). Therefore, it is likely that the secondary reconnection associated with coalescence is electron-only magnetic reconnection, which certainly deserves a detailed study.

Data availability. The measurements from Mio/MEA and MPO/-MAG analyzed in this study are available in the supporting information. The data archiving is underway. Mio/MEA data are available in the Supplement of this article. MPO/MAG data is available in the supplement of this article. The OMNI dataset is publicly available at https://omniweb.gsfc.nasa.gov/ (King and Papitashvili, 2005).

Supplement. The supplement related to this article is available online at: https://doi.org/10.5194/angeo-40-217-2022-supplement.

Author contributions. WS led the work, identified the events, conducted the data analysis of the dataset, and wrote the manuscript. WS, JAS, and RN jointly designed the work. DH and JZDM provided knowledge of the MPO/MAG instrument and the MPO/MAG data. SA and NA provided knowledge of the Mio/MEA instrument and the Mio/MEA data. KJT provided Fig. 3 and the relevant descriptions. JZ performed force-free fittings of the flux ropes. All the authors discussed and contributed to the manuscript.

Competing interests. The contact author has declared that neither they nor their co-authors have any competing interests.

Disclaimer. Publisher's note: Copernicus Publications remains neutral with regard to jurisdictional claims in published maps and institutional affiliations.

Acknowledgements. The BepiColombo project is supported by ESA and JAXA. MEA data analysis was performed with the CL software developed by Emmanuel Penou at IRAP and the AMDA science analysis system provided by the Centre de Données de la Physique des Plasmas (CDPP) supported by CNRS, CNES, Observatoire de Paris, and Université Paul Sabatier, Toulouse. Weijie Sun thanks Gangkai Poh for helpful discussions.

Financial support. This research has been supported by NASA grants NNX16AJ67G, 80NSSC21K0052, 80NSSC21M0364 and 80NSSC18K1137. The research at University of Colorado, Boulder (Karlheinz J. Trattner) has been supported by NASA grants NNG04EB99C and 80NSSC20K0688. Nicolas Andre and Sae Aizawa were supported by CNES for the BepiColombo mission.

Review statement. This paper was edited by Anna Milillo and reviewed by three anonymous referees.

References

Akhavan-Tafti, M., Slavin, J. A., Le, G., Eastwood, J. P., Strangeway, R. J., Russell, C. T., Nakamura, R., Baumjohann, W., Torbert, R. B., Giles, B. L., Gershman, D. J., and Burch, J. L.: MMS Examination of FTEs at the Earth's Subsolar Magnetopause, J. Geophys. Res.-Space, 123, 1224–1241, https://doi.org/10.1002/2017JA024681, 2018.

Belenkaya, E. S.: Reconnection modes for near-radial interplanetary magnetic field, J. Geophys. Res.-Space, 103, 26487–26494, https://doi.org/10.1029/98JA02270, 1998.

Benkhoff, J., van Casteren, J., Hayakawa, H., Fujimoto, M., Laakso, H., Novara, M., Ferri, P., Middleton, H. R., and Ziethe, R.:

BepiColombo—Comprehensive exploration of Mercury: Mission overview and science goals, Planet. Space Sci., 58, 2–20, https://doi.org/10.1016/j.pss.2009.09.020, 2010.

Biskamp, D. and Welter, H.: Coalescence of Magnetic Islands, Phys. Rev. Lett., 44, 1069–1072, https://doi.org/10.1103/PhysRevLett.44.1069, 1980.

Burch, J. L., Moore, T. E., Torbert, R. B., and Giles, B. L.: Magnetospheric Multiscale Overview and Science Objectives, Space Sci. Rev., 199, 5–21, https://doi.org/10.1007/s11214-015-0164-9, 2016.

Burlaga, L. F.: Magnetic clouds and force-free fields with constant alpha, J. Geophys. Res.-Space, 93, 7217–7224, https://doi.org/10.1029/JA093iA07p07217, 1988.

Califano, F., Cerri, S. S., Faganello, M., Laveder, D., Sisti, M., and Kunz, M. W.: Electron-Only Reconnection in Plasma Turbulence, Frontiers in Physics, 8, 317, https://doi.org/10.3389/fphy.2020.00317, 2020.

Dorelli, J. C. and Bhattacharjee, A.: On the generation and topology of flux transfer events, J. Geophys. Res.-Space, 114, A06213, https://doi.org/10.1029/2008JA013410, 2009.

Drake, J. F., Swisdak, M., Che, H., and Shay, M. A.: Electron acceleration from contracting magnetic islands during reconnection, Nature, 443, 553, https://doi.org/10.1038/nature05116, 2006.

Dungey, J. W.: Interplanetary Magnetic Field and the Auroral Zones, Phys. Rev. Lett., 6, 47–48, https://doi.org/10.1103/PhysRevLett.6.47, 1961.

Fear, R. C., Trenchi, L., Coxon, J. C., and Milan, S. E.: How Much Flux Does a Flux Transfer Event Transfer?, J. Geophys. Res.-Space, 122, 12,310-312,327, https://doi.org/10.1002/2017JA024730, 2017.

Fermo, R. L., Drake, J. F., Swisdak, M., and Hwang, K. J.: Comparison of a statistical model for magnetic islands in large current layers with Hall MHD simulations and Cluster FTE observations, J. Geophys. Res.-Space, 116, A09226, https://doi.org/10.1029/2010JA016271, 2011.

Fuselier, S. A. and Lewis, W. S.: Properties of Near-Earth Magnetic Reconnection from In-Situ Observations, Space Sci. Rev., 160, 95, https://doi.org/10.1007/s11214-011-9820-x, 2011.

Gou, X. C., Shi, Q. Q., Tian, A. M., Sun, W. J., Dunlop, M. W., Fu, S. Y., Zong, Q. G., Facskó, G., Nowada, M., Pu, Z. Y., Mailyan, B., Xiao, T., and Shen, X. C.: Solar wind plasma entry observed by cluster in the high-latitude magnetospheric lobes, J. Geophys. Res.-Space, 121, 4135–4144, https://doi.org/10.1002/2015JA021578, 2016.

Heyner, D., Auster, H. U., Fornaçon, K. H., Carr, C., Richter, I., Mieth, J. Z. D., Kolhey, P., Exner, W., Motschmann, U., Baumjohann, W., Matsuoka, A., Magnes, W., Berghofer, G., Fischer, D., Plaschke, F., Nakamura, R., Narita, Y., Delva, M., Volwerk, M., Balogh, A., Dougherty, M., Horbury, T., Langlais, B., Mandea, M., Masters, A., Oliveira, J. S., Sánchez-Cano, B., Slavin, J. A., Vennerstrøm, S., Vogt, J., Wicht, J., and Glassmeier, K. H.: The BepiColombo Planetary Magnetometer MPO-MAG: What Can We Learn from the Hermean Magnetic Field?, Space Sci. Rev., 217, 52, https://doi.org/10.1007/s11214-021-00822-x, 2021.

Hoilijoki, S., Ganse, U., Pfau-Kempf, Y., Cassak, P. A., Walsh, B. M., Hietala, H., von Alfthan, S., and Palmroth, M.: Reconnection rates and X line motion at the magnetopause: Global 2D-3V hybrid-Vlasov simulation results, J. Geophys. Res.-Space, 122, 2877–2888, https://doi.org/10.1002/2016JA023709, 2017.

Imber, S. M., Slavin, J. A., Boardsen, S. A., Anderson, B. J., Korth, H., McNutt Jr., R. L., and Solomon, S. C.: MESSENGER observations of large dayside flux transfer events: Do they drive Mercury's substorm cycle?, J. Geophys. Res.-Space, 119, 5613–5623, https://doi.org/10.1002/2014ja019884, 2014.

Jasinski, J. M., Slavin, J. A., Arridge, C. S., Poh, G., Jia, X., Sergis, N., Coates, A. J., Jones, G. H., and Waite Jr., J. H.: Flux transfer event observation at Saturn's dayside magnetopause by the Cassini spacecraft, Geophys. Res. Lett., 43, 6713–6723, https://doi.org/10.1002/2016GL069260, 2016.

Jasinski, J. M., Akhavan-Tafti, M., Sun, W., Slavin, J. A., Coates, A. J., Fuselier, S. A., Sergis, N., and Murphy, N.: Flux Transfer Events at a Reconnection-Suppressed Magnetopause: Cassini Observations at Saturn, J. Geophys. Res.-Space, 126, e2020JA028786, https://doi.org/10.1029/2020JA028786, 2021.

Kacem, I., Jacquey, C., Génot, V., Lavraud, B., Vernisse, Y., Marchaudon, A., Le Contel, O., Breuillard, H., Phan, T. D., Hasegawa, H., Oka, M., Trattner, K. J., Farrugia, C. J., Paulson, K., Eastwood, J. P., Fuselier, S. A., Turner, D., Eriksson, S., Wilder, F., Russell, C. T., Øieroset, M., Burch, J., Graham, D. B., Sauvaud, J. A., Avanov, L., Chandler, M., Coffey, V., Dorelli, J., Gershman, D. J., Giles, B. L., Moore, T. E., Saito, Y., Chen, L. J., and Penou, E.: Magnetic Reconnection at a Thin Current Sheet Separating Two Interlaced Flux Tubes at the Earth's Magnetopause, J. Geophys. Res.-Space, 123, 1779–1793, https://doi.org/10.1002/2017JA024537, 2018.

Khrabrov, A. V. and Sonnerup, B. U. Ö.: Error estimates for minimum variance analysis, J. Geophys. Res.-Space, 103, 6641–6651, https://doi.org/10.1029/97JA03731, 1998.

King, J. H. and Papitashvili, N. E.: Solar wind spatial scales in and comparisons of hourly Wind and ACE plasma and magnetic field data, J. Geophys. Res.-Space, 110, A02104, https://doi.org/10.1029/2004ja010649, 2005.

Kivelson, M. G. and Khurana, K. K.: Models of flux ropes embedded in a harris neutral sheet: Force-free solutions in low and high beta plasmas, J. Geophys. Res.-Space, 100, 23637–23645, https://doi.org/10.1029/95JA01548, 1995.

Kuo, H., Russell, C. T., and Le, G.: Statistical studies of flux transfer events, J. Geophys. Res.-Space, 100, 3513–3519, https://doi.org/10.1029/94JA02498, 1995.

Lai, H. R., Wei, H. Y., Russell, C. T., Arridge, C. S., and Dougherty, M. K.: Reconnection at the magnetopause of Saturn: Perspective from FTE occurrence and magnetosphere size, J. Geophys. Res.-Space, 117, A05222, https://doi.org/10.1029/2011ja017263, 2012.

Lee, L. C. and Fu, Z. F.: A theory of magnetic flux transfer at the Earth's magnetopause, Geophys. Res. Lett., 12, 105–108, https://doi.org/10.1029/GL012i002p00105, 1985.

Lee, L. C., Ma, Z. W., Fu, Z. F., and Otto, A.: Topology of magnetic flux ropes and formation of fossil flux transfer events and boundary layer plasmas, J. Geophys. Res.-Space, 98, 3943–3951, https://doi.org/10.1029/92JA02203, 1993.

Lepping, R. P., Jones, J. A., and Burlaga, L. F.: Magnetic field structure of interplanetary magnetic clouds at 1 AU, J. Geophys. Res.-Space, 95, 11957–11965, https://doi.org/10.1029/JA095iA08p11957, 1990.

Lockwood, M., Cowley, S. W. H., Smith, M. F., Rijnbeek, R. P., and Elphic, R. C.: The contribution of flux transfer

events to convection, Geophys. Res. Lett., 22, 1185–1188, https://doi.org/10.1029/95gl01008, 1995.

Luhmann, J. G., Walker, R. J., Russell, C. T., Crooker, N. U., Spreiter, J. R., and Stahara, S. S.: Patterns of potential magnetic field merging sites on the dayside magnetopause, J. Geophys. Res.-Space, 89, 1739–1742, https://doi.org/10.1029/JA089iA03p01739, 1984.

Lundquist, S.: Magnetohydrostatic fields, Ark. Fys., 2, 361–365, 1950.

Mangano, V., Dósa, M., Fränz, M., Milillo, A., Oliveira, J. S., Lee, Y. J., McKenna-Lawlor, S., Grassi, D., Heyner, D., Kozyrev, A. S., Peron, R., Helbert, J., Besse, S., de la Fuente, S., Montagnon, E., Zender, J., Volwerk, M., Chaufray, J.-Y., Slavin, J. A., Krüger, H., Maturilli, A., Cornet, T., Iwai, K., Miyoshi, Y., Lucente, M., Massetti, S., Schmidt, C. A., Dong, C., Quarati, F., Hirai, T., Varsani, A., Belyaev, D., Zhong, J., Kilpua, E. K. J., Jackson, B. V., Odstrcil, D., Plaschke, F., Vainio, R., Jarvinen, R., Ivanovski, S. L., Madár, Á., Erdős, G., Plainaki, C., Alberti, T., Aizawa, S., Benkhoff, J., Murakami, G., Quemerais, E., Hiesinger, H., Mitrofanov, I. G., Iess, L., Santoli, F., Orsini, S., Lichtenegger, H., Laky, G., Barabash, S., Moissl, R., Huovelin, J., Kasaba, Y., Saito, Y., Kobayashi, M., and Baumjohann, W.: BepiColombo Science Investigations During Cruise and Flybys at the Earth, Venus and Mercury, Space Sci. Rev., 217, 23, https://doi.org/10.1007/s11214-021-00797-9, 2021.

Milillo, A., Fujimoto, M., Murakami, G., Benkhoff, J., Zender, J., Aizawa, S., Dósa, M., Griton, L., Heyner, D., Ho, G., Imber, S. M., Jia, X., Karlsson, T., Killen, R. M., Laurenza, M., Lindsay, S. T., McKenna-Lawlor, S., Mura, A., Raines, J. M., Rothery, D. A., André, N., Baumjohann, W., Berezhnoy, A., Bourdin, P. A., Bunce, E. J., Califano, F., Deca, J., de la Fuente, S., Dong, C., Grava, C., Fatemi, S., Henri, P., Ivanovski, S. L., Jackson, B. V., James, M., Kallio, E., Kasaba, Y., Kilpua, E., Kobayashi, M., Langlais, B., Leblanc, F., Lhotka, C., Mangano, V., Martindale, A., Massetti, S., Masters, A., Morooka, M., Narita, Y., Oliveira, J. S., Odstrcil, D., Orsini, S., Pelizzo, M. G., Plainaki, C., Plaschke, F., Sahraoui, F., Seki, K., Slavin, J. A., Vainio, R., Wurz, P., Barabash, S., Carr, C. M., Delcourt, D., Glassmeier, K. H., Grande, M., Hirahara, M., Huovelin, J., Korablev, O., Kojima, H., Lichtenegger, H., Livi, S., Matsuoka, A., Moissl, R., Moncuquet, M., Muinonen, K., Quèmerais, E., Saito, Y., Yagitani, S., Yoshikawa, I., and Wahlund, J. E.: Investigating Mercury's Environment with the Two-Spacecraft BepiColombo Mission, Space Sci. Rev., 216, 93, https://doi.org/10.1007/s11214-020-00712-8, 2020.

Montag, P., Egedal, J., Lichko, E., and Wetherton, B.: Impact of compressibility and a guide field on Fermi acceleration during magnetic island coalescence, Phys. Plasmas, 24, 062906, https://doi.org/10.1063/1.4985302, 2017.

Murakami, G., Hayakawa, H., Ogawa, H., Matsuda, S., Seki, T., Kasaba, Y., Saito, Y., Yoshikawa, I., Kobayashi, M., Baumjohann, W., Matsuoka, A., Kojima, H., Yagitani, S., Moncuquet, M., Wahlund, J.-E., Delcourt, D., Hirahara, M., Barabash, S., Korablev, O., and Fujimoto, M.: Mio—First Comprehensive Exploration of Mercury's Space Environment: Mission Overview, Space Sci. Rev., 216, 113, https://doi.org/10.1007/s11214-020-00733-3, 2020.

Øieroset, M., Phan, T. D., Haggerty, C., Shay, M. A., Eastwood, J. P., Gershman, D. J., Drake, J. F., Fujimoto, M., Ergun, R. E., Mozer, F. S., Oka, M., Torbert, R. B., Burch, J. L., Wang, S., Chen, L. J., Swisdak, M., Pollock, C., Dorelli, J. C., Fuselier, S. A., Lavraud, B., Giles, B. L., Moore, T. E., Saito, Y., Avanov, L. A., Paterson, W., Strangeway, R. J., Russell, C. T., Khotyaintsev, Y., Lindqvist, P. A., and Malakit, K.: MMS observations of large guide field symmetric reconnection between colliding reconnection jets at the center of a magnetic flux rope at the magnetopause, Geophys. Res. Lett., 43, 5536–5544, https://doi.org/10.1002/2016GL069166, 2016.

Paschmann, G., Haerendel, G., Papamastorakis, I., Sckopke, N., Bame, S. J., Gosling, J. T., and Russell, C. T.: Plasma and magnetic field characteristics of magnetic flux transfer events, J. Geophys. Res.-Space, 87, 2159–2168, https://doi.org/10.1029/JA087iA04p02159, 1982.

Phan, T. D., Sonnerup, B. U. Ö., and Lin, R. P.: Fluid and kinetics signatures of reconnection at the dawn tail magnetopause: Wind observations, J. Geophys. Res.-Space, 106, 25489–25501, https://doi.org/10.1029/2001JA900054, 2001.

Phan, T. D., Eastwood, J. P., Shay, M. A., Drake, J. F., Sonnerup, B. U. Ö., Fujimoto, M., Cassak, P. A., Øieroset, M., Burch, J. L., Torbert, R. B., Rager, A. C., Dorelli, J. C., Gershman, D. J., Pollock, C., Pyakurel, P. S., Haggerty, C. C., Khotyaintsev, Y., Lavraud, B., Saito, Y., Oka, M., Ergun, R. E., Retino, A., Le Contel, O., Argall, M. R., Giles, B. L., Moore, T. E., Wilder, F. D., Strangeway, R. J., Russell, C. T., Lindqvist, P. A., and Magnes, W.: Electron magnetic reconnection without ion coupling in Earth's turbulent magnetosheath, Nature, 557, 202–206, https://doi.org/10.1038/s41586-018-0091-5, 2018.

Pi, G., Shue, J.-H., Grygorov, K., Li, H.-M., Němeček, Z., Šafránková, J., Yang, Y.-H., and Wang, K.: Evolution of the magnetic field structure outside the magnetopause under radial IMF conditions, J. Geophys. Res.-Space, 122, 4051–4063, https://doi.org/10.1002/2015JA021809, 2017.

Poh, G., Slavin, J. A., Lu, S., Le, G., Ozturk, D. S., Sun, W.-J., Zou, S., Eastwood, J. P., Nakamura, R., Baumjohann, W., Russell, C. T., Gershman, D. J., Giles, B. L., Pollock, C. J., Moore, T. E., Torbert, R. B., and Burch, J. L.: Dissipation of Earthward Propagating Flux Rope Through Re-reconnection with Geomagnetic Field: An MMS Case Study, J. Geophys. Res.-Space, 124, 7477–7493, https://doi.org/10.1029/2018JA026451, 2019.

Pritchett, P. L. and Coroniti, F. V.: Three-dimensional collisionless magnetic reconnection in the presence of a guide field, J. Geophys. Res.-Space, 109, A01220, https://doi.org/10.1029/2003ja009999, 2004.

Raeder, J.: Flux Transfer Events: 1. generation mechanism for strong southward IMF, Ann. Geophys., 24, 381–392, https://doi.org/10.5194/angeo-24-381-2006, 2006.

Ricci, P., Brackbill, J. U., Daughton, W., and Lapenta, G.: Collisionless magnetic reconnection in the presence of a guide field, Phys. Plasmas, 11, 4102–4114, https://doi.org/10.1063/1.1768552, 2004.

Rijnbeek, R. P., Cowley, S. W. H., Southwood, D. J., and Russell, C. T.: A survey of dayside flux transfer events observed by ISEE 1 and 2 magnetometers, J. Geophys. Res.-Space, 89, 786–800, https://doi.org/10.1029/JA089iA02p00786, 1984.

Russell, C. T. and Elphic, R. C.: Initial ISEE magnetometer results: magnetopause observations, Space Sci. Rev., 22, 681–715, https://doi.org/10.1007/BF00212619, 1978.

Russell, C. T. and Walker, R. J.: Flux transfer events at Mercury, J. Geophys. Res.-Space, 90, 11067–11074, https://doi.org/10.1029/JA090iA11p11067, 1985.

Saito, Y., Delcourt, D., Hirahara, M., Barabash, S., André, N., Takashima, T., Asamura, K., Yokota, S., Wieser, M., Nishino, M. N., Oka, M., Futaana, Y., Harada, Y., Sauvaud, J.-A., Louarn, P., Lavraud, B., Génot, V., Mazelle, C., Dandouras, I., Jacquey, C., Aoustin, C., Barthe, A., Cadu, A., Fedorov, A., Frezoul, A.-M., Garat, C., Le Comte, E., Lee, Q.-M., Médale, J.-L., Moirin, D., Penou, E., Petiot, M., Peyre, G., Rouzaud, J., Séran, H.-C., Němec?ek, Z., S?afránková, J., Marcucci, M. F., Bruno, R., Consolini, G., Miyake, W., Shinohara, I., Hasegawa, H., Seki, K., Coates, A. J., Leblanc, F., Verdeil, C., Katra, B., Fontaine, D., Illiano, J.-M., Berthelier, J.-J., Techer, J.-D., Fraenz, M., Fischer, H., Krupp, N., Woch, J., Bührke, U., Fiethe, B., Michalik, H., Matsumoto, H., Yanagimachi, T., Miyoshi, Y., Mitani, T., Shimoyama, M., Zong, Q., Wurz, P., Andersson, H., Karlsson, S., Holmström, M., Kazama, Y., Ip, W.-H., Hoshino, M., Fujimoto, M., Terada, N., Keika, K., and BepiColombo Mio, M. T.: Preflight Calibration and Near-Earth Commissioning Results of the Mercury Plasma Particle Experiment (MPPE) Onboard MMO (Mio), Space Sci. Rev., 217, 70, https://doi.org/10.1007/s11214-021-00839-2, 2021.

Saunders, M. A., Russell, C. T., and Sckopke, N.: Flux transfer events: Scale size and interior structure, Geophys. Res. Lett., 11, 131–134, https://doi.org/10.1029/GL011i002p00131, 1984.

Sauvaud, J. A., Fedorov, A., Aoustin, C., Seran, H. C., Le Comte, E., Petiot, M., Rouzaud, J., Saito, Y., Dandouras, J., Jacquey, C., Louarn, P., Mazelle, C., and Médale, J. L.: The Mercury Electron Analyzers for the Bepi Colombo mission, Adv. Space Res., 46, 1139–1148, https://doi.org/10.1016/j.asr.2010.05.022, 2010.

Schindler, K., Pfirsch, D., and Wobig, H.: Stability of two-dimensional collision-free plasmas, Plasma Physics, 15, 1165–1184, https://doi.org/10.1088/0032-1028/15/12/001, 1973.

Shi, Q. Q., Zong, Q. G., Zhang, H., Pu, Z. Y., Fu, S. Y., Xie, L., Wang, Y. F., Chen, Y., Li, L., Xia, L. D., Liu, Z. X., Fazakerley, A. N., Reme, H., and Lucek, E.: Cluster observations of the entry layer equatorward of the cusp under northward interplanetary magnetic field, J. Geophys. Res.-Space, 114, A12219, https://doi.org/10.1029/2009JA014475, 2009.

Shi, Q. Q., Zong, Q. G., Fu, S. Y., Dunlop, M. W., Pu, Z. Y., Parks, G. K., Wei, Y., Li, W. H., Zhang, H., Nowada, M., Wang, Y. B., Sun, W. J., Xiao, T., Reme, H., Carr, C., Fazakerley, A. N., and Lucek, E.: Solar wind entry into the high-latitude terrestrial magnetosphere during geomagnetically quiet times, Nat. Commun., 4, 1466, https://doi.org/10.1038/ncomms2476, 2013.

Slavin, J. A., Acuña, M. H., Anderson, B. J., Baker, D. N., Benna, M., Boardsen, S. A., Gloeckler, G., Gold, R. E., Ho, G. C., Korth, H., Krimigis, S. M., McNutt, R. L., Raines, J. M., Sarantos, M., Schriver, D., Solomon, S. C., Trávníček, P., and Zurbuchen, T. H.: MESSENGER Observations of Magnetic Reconnection in Mercury's Magnetosphere, Science, 324, 606, https://doi.org/10.1126/science.1172011, 2009.

Slavin, J. A., Lepping, R. P., Wu, C.-C., Anderson, B. J., Baker, D. N., Benna, M., Boardsen, S. A., Killen, R. M., Korth, H., Krimigis, S. M., McClintock, W. E., McNutt Jr., R. L., Sarantos, M., Schriver, D., Solomon, S. C., Trávníček, P., and Zurbuchen, T. H.: MESSENGER observations of large flux transfer events at Mercury, Geophys. Res. Lett., 37, L02105, https://doi.org/10.1029/2009gl041485, 2010.

Slavin, J. A., Imber, S. M., Boardsen, S. A., DiBraccio, G. A., Sundberg, T., Sarantos, M., Nieves-Chinchilla, T., Szabo, A., Anderson, B. J., Korth, H., Zurbuchen, T. H., Raines, J. M., Johnson, C. L., Winslow, R. M., Killen, R. M., McNutt Jr., R. L., and Solomon, S. C.: MESSENGER observations of a flux-transfer-event shower at Mercury, J. Geophys. Res.-Space, 117, A00M06, https://doi.org/10.1029/2012ja017926, 2012.

Song, P. and Russell, C. T.: Model of the formation of the low-latitude boundary layer for strongly northward interplanetary magnetic field, J. Geophys. Res.-Space, 97, 1411–1420, https://doi.org/10.1029/91JA02377, 1992.

Sonnerup, B. U. Ö.: Magnetopause reconnection rate, J. Geohys. Res., 79, 1546–1549, https://doi.org/10.1029/JA079i010p01546, 1974.

Sonnerup, B. U. Ö. and Cahill Jr., L. J.: Magnetopause structure and attitude from Explorer 12 observations, J. Geohys. Res., 72, 171–183, https://doi.org/10.1029/JZ072i001p00171, 1967.

Sonnerup, B. U. Ö. and Scheible, M.: Minimum and maximum variance analysis, in: Analysis methods for multi-spacecraft data, edited by: Paschmann, G. and Daly, P. W., ESA Publication, Noordwijk, Netherlands, 185–220, 1998.

Sonnerup, B. U. Ö., Paschmann, G., Papamastorakis, I., Sckopke, N., Haerendel, G., Bame, S. J., Asbridge, J. R., Gosling, J. T., and Russell, C. T.: Evidence for magnetic field reconnection at the Earth's magnetopause, J. Geophys. Res.-Space, 86, 10049–10067, https://doi.org/10.1029/JA086iA12p10049, 1981.

Stawarz, J. E., Eastwood, J. P., Phan, T. D., Gingell, I. L., Shay, M. A., Burch, J. L., Ergun, R. E., Giles, B. L., Gershman, D. J., Contel, O. L., Lindqvist, P. A., Russell, C. T., Strangeway, R. J., Torbert, R. B., Argall, M. R., Fischer, D., Magnes, W., and Franci, L.: Properties of the Turbulence Associated with Electron-only Magnetic Reconnection in Earth's Magnetosheath, Astrophys J., 877, L37, https://doi.org/10.3847/2041-8213/ab21c8, 2019.

Sun, W., Dewey, R. M., Aizawa, S., Huang, J., Slavin, J. A., Fu, S., Wei, Y., and Bowers, C. F.: Review of Mercury's dynamic magnetosphere: Post-MESSENGER era and comparative magnetospheres, Sci. China Earth Sci., 65, 25–74, https://doi.org/10.1007/s11430-021-9828-0, 2022.

Sun, W. J., Slavin, J. A., Smith, A. W., Dewey, R. M., Poh, G. K., Jia, X., Raines, J. M., Livi, S., Saito, Y., Gershman, D. J., DiBraccio, G. A., Imber, S. M., Guo, J. P., Fu, S. Y., Zong, Q. G., and Zhao, J. T.: Flux Transfer Event Showers at Mercury: Dependence on Plasma β and Magnetic Shear and Their Contribution to the Dungey Cycle, Geophys. Res. Lett., 47, e2020GL089784, https://doi.org/10.1029/2020GL089784, 2020a.

Sun, W. J., Slavin, J. A., Dewey, R. M., Chen, Y., DiBraccio, G. A., Raines, J. M., Jasinski, J. M., Jia, X., and Akhavan-Tafti, M.: MESSENGER Observations of Mercury's Nightside Magnetosphere Under Extreme Solar Wind Conditions: Reconnection-Generated Structures and Steady Convection, J. Geophys. Res.-Space, 125, e2019JA027490, https://doi.org/10.1029/2019ja027490, 2020b.

Tang, B. B., Wang, C., and Li, W. Y.: The magnetosphere under the radial interplanetary magnetic field: A numerical study, J. Geophys. Res.-Space, 118, 7674–7682, https://doi.org/10.1002/2013JA019155, 2013.

Toledo-Redondo, S., Hwang , K.-J., Escoubet , C. P., Lavraud , B., Fornieles , J., Aunai , N., Fear , R. C., Dargent , J., Fu, H. S., Fuselier , S. A., Genestreti , K. J., Khotyaintsev , Y. V., Li, W. Y., Norgren , C., and Phan , T. D.: Solar Wind—Magnetosphere Coupling During Radial Interplanetary Magnetic Field Conditions: Simultaneous Multi-Point Observations, J. Geophys. Res.-Space, 126, e2021JA029506, https://doi.org/10.1029/2021JA029506, 2021.

Trattner, K. J., Mulcock, J. S., Petrinec, S. M., and Fuselier, S. A.: Probing the boundary between antiparallel and component reconnection during southward interplanetary magnetic field conditions, J. Geophys. Res.-Space, 112, A08210, https://doi.org/10.1029/2007JA012270, 2007.

Trattner, K. J., Petrinec, S. M., Fuselier, S. A., and Phan, T. D.: The location of reconnection at the magnetopause: Testing the maximum magnetic shear model with THEMIS observations, J. Geophys. Res.-Space, 117, A01201, https://doi.org/10.1029/2011JA016959, 2012.

Trattner, K. J., Burch, J. L., Ergun, R., Eriksson, S., Fuselier, S. A., Giles, B. L., Gomez, R. G., Grimes, E. W., Lewis, W. S., Mauk, B., Petrinec, S. M., Russell, C. T., Strangeway, R. J., Trenchi, L., and Wilder, F. D.: The MMS Dayside Magnetic Reconnection Locations During Phase 1 and Their Relation to the Predictions of the Maximum Magnetic Shear Model, J. Geophys. Res.-Space, 122, 11991–12005, https://doi.org/10.1002/2017JA024488, 2017.

Trattner, K. J., Fuselier, S. A., Petrinec, S. M., Burch, J. L., Ergun, R., and Grimes, E. W.: Long and Active Magnetopause Reconnection X-Lines During Changing IMF Conditions, J. Geophys. Res.-Space, 126, e2020JA028926, https://doi.org/10.1029/2020JA028926, 2021.

Walker, R. J. and Russell, C. T.: Flux transfer events at the Jovian magnetopause, J. Geophys. Res.-Space, 90, 7397–7404, https://doi.org/10.1029/JA090iA08p07397, 1985.

Wang, Y. L., Elphic, R. C., Lavraud, B., Taylor, M. G. G. T., Birn, J., Raeder, J., Russell, C. T., Kawano, H., Zong, Q.-G., Zhang, H., Zhang, X. X., and Friedel, R. H.: Initial results of high-latitude magnetopause and low-latitude flank flux transfer events from 3 years of Cluster observations, J. Geophys. Res.-Space, 110, A11221, https://doi.org/10.1029/2005JA011150, 2005.

Wang, Y. L., Elphic, R. C., Lavraud, B., Taylor, M. G. G. T., Birn, J., Russell, C. T., Raeder, J., Kawano, H., and Zhang, X. X.: Dependence of flux transfer events on solar wind conditions from 3 years of Cluster observations, J. Geophys. Res.-Space, 111, A04224, https://doi.org/10.1029/2005JA011342, 2006.

Zhang, H., Khurana, K. K., Kivelson, M. G., Angelopoulos, V., Pu, Z. Y., Zong, Q.-G., Liu, J., and Zhou, X.-Z.: Modeling a force-free flux transfer event probed by multiple Time History of Events and Macroscale Interactions during Substorms (THEMIS) spacecraft, J. Geophys. Res.-Space, 113, A00C05, https://doi.org/10.1029/2008ja013451, 2008.

Zhao, J. T., Sun, W.-J., Zong, Q. G., Slavin, J. A., Zhou, X. Z., Dewey, R. M., Poh, G. K., and Raines, J. M.: A Statistical Study of the Force Balance and Structure in the Flux Ropes in Mercury's Magnetotail, J. Geophys. Res.-Space, 124, 5143–5157, https://doi.org/10.1029/2018ja026329, 2019.

Zhong, J., Wei, Y., Lee, L. C., He, J. S., Slavin, J. A., Pu, Z. Y., Zhang, H., Wang, X. G., and Wan, W. X.: Formation of Macroscale Flux Transfer Events at Mercury, Astrophys J., 893, L18, https://doi.org/10.3847/2041-8213/ab8566, 2020.

Zhou, M., Berchem, J., Walker, R. J., El-Alaoui, M., Deng, X., Cazzola, E., Lapenta, G., Goldstein, M. L., Paterson, W. R., Pang, Y., Ergun, R. E., Lavraud, B., Liang, H., Russell, C. T., Strangeway, R. J., Zhao, C., Giles, B. L., Pollock, C. J., Lindqvist, P. A., Marklund, G., Wilder, F. D., Khotyaintsev, Y. V., Torbert, R. B., and Burch, J. L.: Coalescence of Macroscopic Flux Ropes at the Subsolar Magnetopause: Magnetospheric Multiscale Observations, Phys. Rev. Lett., 119, 055101, https://doi.org/10.1103/PhysRevLett.119.055101, 2017.